NIR-Emission

Oxidative Coupling

Emission in water

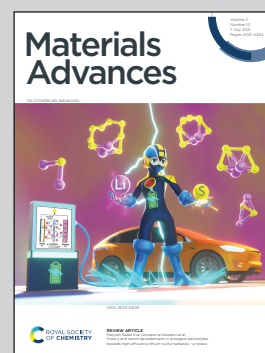Two-Photon Properties

Photo-Stability

Bioimaging

Showcasing research from Professor Andreu's laboratory, Department of Organic Chemistry-INMA, University of Zaragoza-CSIC, Aragón, Spain and Professor Ruiz Delgado's laboratory, Department of Physical Chemistry, University of Malaga, Andalucía, Spain.

V-shaped pyranylidene/triphenylamine-based chromophores with enhanced photophysical, electrochemical and nonlinear optical properties

A comprehensive study of two chromophores based on 4H-pyranylidene moiety as a part of the π-conjugated spacer is developed. Triphenylamine donor units and tricarbonitrile-based electron-accepting groups complete these V-shaped architectures. The two compounds exhibit near-infrared fluorescence, large Stokes shift, enhanced emission in tetrahydrofuran/water mixtures and good photostability. The dimerization of triphenylamine groups upon electrochemical oxidation highlights their peculiar electrochemical behavior and film formation capabilities. High molecular first hyperpolarizabilities and two-photon absorption cross-sections were also found. Overall, these chromophores are versatile materials with a myriad of applications, including biological applications.

ROYAL SOCIETY OF CHEMISTRY

rsc.li/materials-advances

PAPER

Check for updates

V-shaped pyranylidene/triphenylamine-based chromophores with enhanced photophysical, electrochemical and nonlinear optical properties†

Sergio Gámez-Valenzuela,[a] David Neusser,[b] Carlos Benitez-Martin, [iD] [cd] Francisco Najera, [iD] [cd] Juan A. Guadix, [iD] [de] Carlos Moreno-Yruela, [iD] [fg] Belén Villacampa, [iD] [h] Rocío Ponce Ortiz, [iD] [a] Sabine Ludwigs, [iD] [b] Raquel Andreu [iD] *[f] and M. Carmen Ruiz Delgado [iD] *[a]

We report the synthesis and comprehensive study of two chromophores based on 4*H*-pyranylidene moiety as a part of the π-conjugated spacer. Triphenylamine (TPA) acts as donor and tricarbonitrile-based electron-accepting groups complete these V-shaped D–A–D architectures (A, acceptor; D, donor). Their electrochemical, photophysical and nonlinear optical properties are analyzed in detail by using a joint experimental and theoretical approach. The two chromophores exhibit near-infrared fluorescence, large Stokes shift, enhanced emission in tetrahydrofuran/water mixtures and good photostability. Additionally, the dimerization of triphenylamine groups to tetraphenylbenzidine (TPB) takes place upon electrochemical and chemical oxidation showing their peculiar electrochemical behavior and film formation capabilities. Interestingly, high molecular first hyperpolarizabilities and two-photon absorption cross-sections were found, highlighting their potential applications in electro-optical devices. Overall, our work demonstrates that these near-infrared (NIR) fluorescent chromophores are versatile materials with a myriad of applications ranging from optoelectronics to biological applications.

[a] *Department of Physical Chemistry, University of Malaga, Campus de Teatinos s/n, 29071, Malaga, Spain. E-mail: carmenrd@uma.es*

[b] *IPOC – Functional Polymers, Institute of Polymer Chemistry, University of Stuttgart, Pfaffenwaldring 55, D-70569 Stuttgart, Germany*

[c] *Departamento de Química Orgánica, Universidad de Málaga-IBIMA, Campus de Teatinos s/n, Málaga 29071, Spain*

[d] *Centro Andaluz de Nanomedicina y Biotecnología-BIONAND, Parque Tecnológico de Andalucía, c/Severo Ochoa, 35, 29590 Campanillas, Málaga 29071, Spain*

[e] *Departamento de Biología Animal, Facultad de Ciencias, Universidad de Málaga-IBIMA, Campus de Teatinos s/n, Málaga 29071, Spain*

[f] *Instituto de Nanociencia y Materiales de Aragón (INMA)-Departamento de Química Orgánica, CSIC-Universidad de Zaragoza, Zaragoza 50009, Spain. E-mail: randreu@unizar.es*

[g] *Center for Biopharmaceuticals & Department of Drug Design and Pharmacology, Faculty of Health and Medical Sciences, University of Copenhagen, Universitetsparken 2, DK-2100 Copenhagen, Denmark*

[h] *Instituto de Nanociencia y Materiales de Aragón (INMA)-Departamento de Física de la Materia Condensada, CSIC-Universidad de Zaragoza, Zaragoza 50009, Spain*

† Electronic supplementary information (ESI) available: Experimental and theoretical details, synthesis, DFT-calculations, photostability, spectroelectrochemistry and chemical doping and 2P-fluorescence spectra/imaging. See DOI: 10.1039/d1ma00415h

Introduction

Organic push–pull molecules represent a subclass of π-conjugated systems that are end-capped with electron donor(s) and electron acceptor(s). The D–π–A arrangement allows the direct interaction of the donor (D) and the acceptor (A) through the π-system, so-called intramolecular charge transfer (ICT). Their versatility and well-defined and tunable structures, which give rise to predictable properties, represent a main advantage keeping them into focus for different applications: nonlinear optics (NLO),[1] dye-sensitized solar cells (DSSCs),[2] bulk-heterojunction solar cells (BHJSCs),[3] organic light-emitting diodes (OLEDs),[4] two-photon absorbers,[5] or near-infrared absorbing dyes (NIR).[6]

In addition to the ordinary linear D–π–A systems, push–pull chromophores may also adopt quadrupolar (D–π–A–π–D or A–π–D–π–A), tripodal (D–(π–A)₃ or A–(π–D)₃) or even more extraordinary arrangements, which may be pictured as uppercase letters (molecules with shape similar to H, V, X or Y).[7] As far as the field of NLO is concerned, non-centrosymmetry is an imperative requirement for applications based on second order processes.[8] On the other hand, for two-photon absorption (2PA) (a third order process) a high degree of π conjugation is desirable. Following the arrangements above mentioned, branching donors and acceptors

to a π-conjugated backbone contributes in a great extent to enhance the 2PA cross-sections. Thus, D–π–D, A–π–A, D–A–D or A–D–A architectures are pointed as ideal platforms for developing two-photon absorption active compounds.[5]

Triphenylamine (TPA) and 4H-pyranylidene are building blocks often used in the design of D–π–A systems in different research areas. Thus, the use of TPA is based on its strong electron donor character and excellent transporting capabilities, together with its special propeller-like structure.[9] Its nonplanar conformation is beneficial for restraining intermolecular aggregation as well as for obtaining amorphous materials. Its electrochemical behavior has been extensively studied due to the dimerization ability as a result of oxidative coupling,[10–13] which is also observed in polymer systems.[14] TPA derivatives have been investigated and applied in a variety of areas, such as organic photovoltaics,[11,15] DSSC and perovskite solar cells,[15] 2PA[16–18] materials or OLEDs.[19]

On the other hand, 4H-pyranylidene can act as a proaromatic donor unit,[20] but also as a part of the π-bridge of a push–pull system, with one C=C bond of the spacer in the ring, and opening the possibility of introducing strong acceptor groups on its 4 position. With this architecture, materials with interesting properties, such as NLO activity[21] or good performance as dyes in DSSCs have been developed.[22]

Furthermore, both entities (TPA and 4H-pyranylidene) have demonstrated to lead to derivatives with large fluorescence yields.[19,23] This fact, together with the possibility of becoming highly emissive upon aggregation in poor solvents[24] and the achievement of large two photon-absorption cross sections[17,25–27] make these type of compounds good candidates for the development of highly efficient probes for biological imaging.[25,28,29]

Within this context, we present a comprenhensive study of two V-shaped D–A–D systems, which have been designed according to this approach: (i) the propeller-like TPA is the donor moiety; (ii) 4H-pyranylidene acts as a part of the π-conjugated bridge; (iii) strong polycyano acceptors like 1,1,3-tricyano-2-phenylpropene[30] and 2-dicyanomethylene-3-cyano-4,5,5-trimethyl-2,5-dihydrofuran (TCF)[31] are attached to the pyran unit (4 position) giving rise to chromophores **1** and **2**, respectively (Fig. 1). The electronic and steric effect of cyano groups is also important in the development of systems with great color tunability and enhanced emission upon aggregation.[24]

The excellent potential of these two conjugated systems in different fields will be studied by means of a complementary experimental and theoretical approach. On the one hand, the prominent ICT from the external branched units to the central acceptor group are expected to provide both second-order NLO and suitable two-photon absorption (2PA) properties; on the other hand, due to the presence of two fluorescent moieties, they will be studied as luminescent materials, paying particular attention to the effect of biological-compatible aqueous solutions on luminescence. Their photostability together with the 2PA fluorescence cell imaging have been investigated. Eventually, and having in mind the electrochemical behavior of TPA derivatives, an extensive study of this aspect has been carried out.
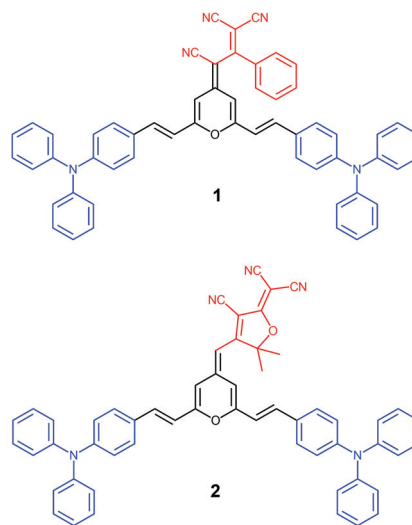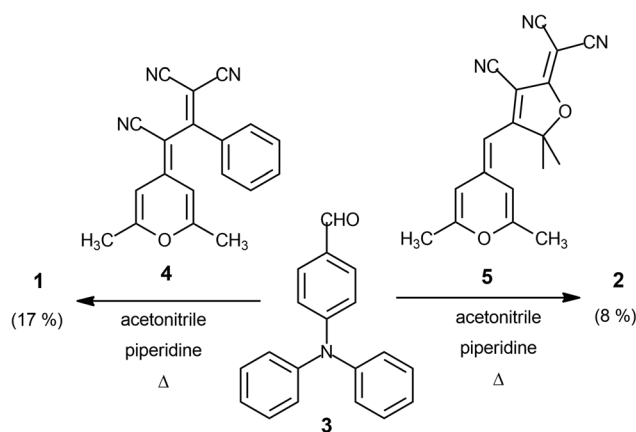

Fig. 1　Chemical structures of the two chromophores under study.

Results and discussion

1.　Synthesis

Target conjugated systems **1** and **2** were prepared by Knœvenagel-type condensation between the commercially available p-diphenylaminobenzaldehyde (**3**) (2 equiv.) and the 2,6-dimethyl-4H-pyran-4-ylidene derivatives **4**[32] and **5**[32] respectively (Scheme 1). Compound **1** was prepared slightly modifying the reaction conditions and purification previously described.[29] In addition to the described characterization, mp, IR and elemental analysis have been also included (see ESI†). The attainment of small amounts of the corresponding mono-substituted derivatives and subsequent repeated chromatographic purification on silica gel (for compound **2**) contribute to explain the fact that chromophores were obtained in low-moderate yields. The analysis of the $^3J_{HH}$ coupling constants allows us to infer that the formed CH=CH bond has an E configuration. It is noteworthy to remark that signals corresponding to aromatic protons are overlapped for both compounds.

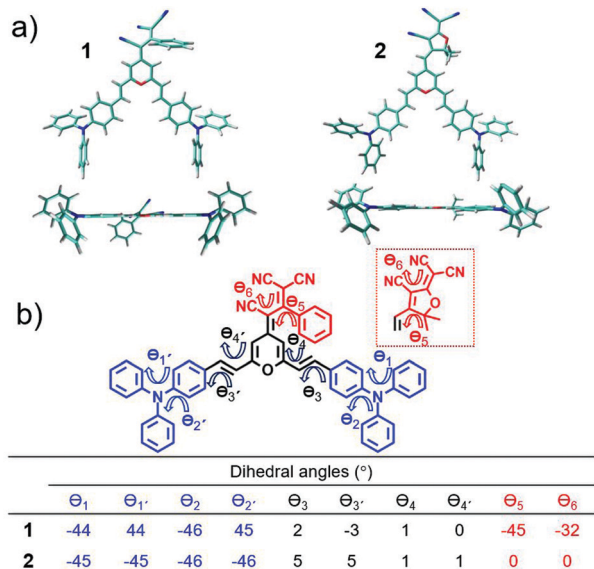
Scheme 1　Synthesis of chromophores **1** and **2**.

Fig. 2 (a) Top and lateral views of the DFT-optimized structures for **1** and **2** systems at the PCM-M06-2X/6-31G** level using CH_2Cl_2 as solvent. (b) DFT-calculated intering dihedral angles (θ) along the conjugated backbones of **1** and **2** using the same level of theory.

Fig. 3 (a) Mülliken atomic charges on various molecular domains and (b) structural parameters for chromophores **1** and **2** calculated at the PCM-M06-2X/6-31G** level using CH_2Cl_2 as solvent.

2. Structural features

Fig. 2 displays the top and lateral views of the DFT-optimized ground-state structures for **1** and **2**. As we observe, the outermost phenyl rings of the TPA units are largely distorted by ∼45° from the rest of the π-conjugated backbone which shows an almost coplanar arrangement; note that very small dihedral angles are predicted between the vinyl-pyran unit and the adjacent phenyl ring, with θ_3, θ_4 and $\theta_{3'}$, $\theta_{4'}$ values of ∼0°–5°. However, when we focus on the distinctive chemical electron-acceptor units, notable geometrical differences are found: (i) in compound **1**, the phenyl and external dicyanovinyl group of the acceptor moiety is appreciably distorted from planarity (with θ_5 and θ_6 values of 45° and 32°, respectively), in good agreement with X-ray structures of other push–pull systems bearing the same acceptor,[29,32] and (ii) the TCF acceptor unit of **2** shows an almost planar disposition with respect to the pyran unit.

We now make use of the Mülliken atomic charges and bond length alternation (BLA) values that allow for a deeper understanding of the ground-state polarization of the chromophores. Note that the BLA values are related to the degree of bond length alternation, δr, which equals 0 for benzene while values ∼0.10 are found in fully quinoid rings.[33] As seen in Fig. 3, the two chromophores exhibit a decreased degree of bond length alternation for pyran (δr = 0.065 for **1** and δr = 0.069 for **2**) and a lengthening of the pyran exocyclic C_4–C_{exo} bond length (1.413 Å for **1** and 1.403 Å for **2**) when compared to that reported for a fully quinoidal 2,2,6,6-tetraphenylbipyranylidene (with δr = 0.11 and C_4–C_{exo} bond length of 1.385 Å)[34] together with less alternated internal phenyl rings when compared to the external ones. These structural parameters reflect a degree of mixing between the neutral form and the charge-separated zwitterionic one with a more (less) aromatized pyran spacer (internal phenyl rings).
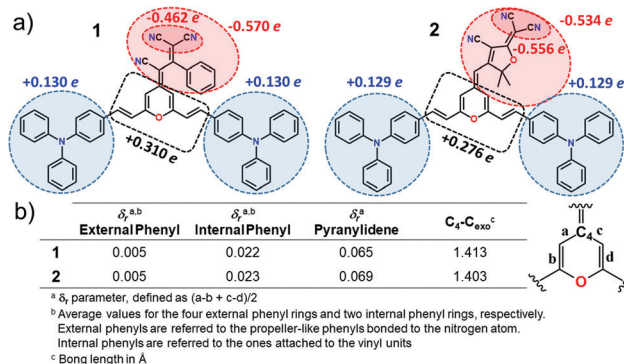
As seen in Fig. 3, Mülliken population analysis confirms these trends indicating a negative charge over the acceptor group (−0.569 e in **1** and −0.534 e in **2**) which is around 2 times higher than the sum of the positive charge over the two TPA donor groups (+0.260 e in **1** and +0.258 e in **2**), while the π-spacer is largely polarized bearing around 70% (+0.310 e in **1** and +0.276 e in **2**) of the total positive charge. Moreover, it is worth highlighting that the positive charge located in the pyran ring (together with vinyl unit) is of the same order[35] or even larger[36,37] to those encountered for other D–π–A derivatives with the 4H-pyranylidene as main donor. Thus, these data account for a significant polarization of the π-conjugated structure in these V-shaped chromophores.

IR and Raman spectra can provide useful information about the degree of charge polarization in the ground state.[38–40] In this sense, the frequency of the $\nu(C\equiv N)$ is very sensitive to the total charge borne by the nitrile groups, downshifting upon ground-state polarization. Indeed, taken the nonconjugated malononitrile $(CH_2(CN)_2)$ as reference, for which the $\nu(C\equiv N)$ band is recorded at 2270 cm^{-1}, the low frequency values for the corresponding IR absorption in our chromophores (at 2213 and 2188 cm^{-1} for **1** and 2217 and 2206 cm^{-1} for **2**, see Fig. 4a) reveal an intramolecular charge-transfer (ICT) from the TPA groups towards the central electron-withdrawing moiety.[41–43] On the other hand, it is interesting to note that the Raman bands in the 1640–1590 cm^{-1} region, which corresponds to $\nu(C=C/C–C)$ stretching of the π-conjugated spacer (vinyl and pyran) and the TPA donor groups, slightly changes on going from **1** to **2** (Fig. 4b and Fig. S5, S6, ESI†). The downshift of the $\nu(C=C)$ mode in the pyran moiety when going from **2** to **1** (from 1639 to 1632 cm^{-1}) can be ascribed to the different electronic nature of the group directly linked to the pyran exocyclic bond (a CH group in **2** and a C(CN) group in **1**) which results in a more positive charge localization over the pyran unit in **1** than in **2** as seen in Fig. 3a. However, a shift towards lower frequencies of the $\nu(C=C)$ stretching on the vinyl groups (from 1622 in **1** to 1619 cm^{-1} in **2**) and a larger negative charge on the peripheral $C(CN)_2$ groups (−0.462 e in **1** to −0.556 e in **2**) is found when comparing **1** with **2**. Theoretical IR and Raman spectra are in good agreement with the experimental results (Fig. S3–S6, ESI†) and the vibrational
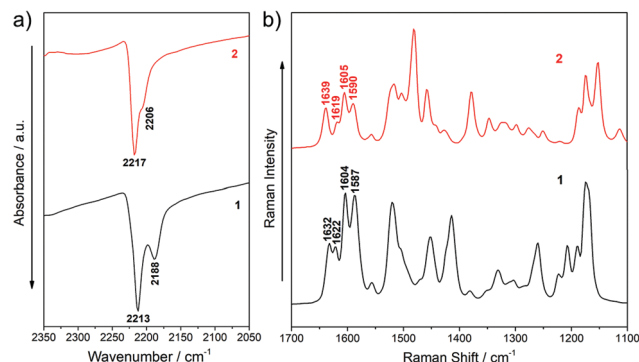
Fig. 4 (a) IR and (b) Raman spectra of chromophores **1** and **2**.

Table 1 Main photophysical properties of compounds **1** and **2**

Compound	Solvent	$\lambda_{abs}{}^{a}$ (nm)	$\lambda_{em}{}^{b}$ (nm)	$E_{g,op}{}^{c}$ (eV)	$\lambda_{em} - \lambda_{abs}$ (nm)	Stokes shift^{d} (cm^{-1})	Φ^{e}
1	CH$_2$Cl$_2$	570	782	1.90	212	4756	0.035
	Toluene	545	665	1.94	120	3311	0.009
2	CH$_2$Cl$_2$	641	784	1.77	143	2846	0.008
	Toluene	594	735	1.76	141	3230	0.002

^{a} Lowest-energy electronic absorption maxima. ^{b} Emission fluorescence maxima. ^{c} Optical band gap estimated from the tangent to the low energy edge of the absorption band. ^{d} Stokes shift as the difference between the wavelength of the emission and absorption maxima. ^{e} Fluorescence emission quantum yield, 15% error.

eigenvectors nicely support the assignments. Overall, these results reveal similar ground-state polarization in both systems with a slightly larger contribution of the charge-separated zwitterionic form in **2** due to the insertion of the TCF acceptor.

3. Photophysical properties

Fig. 5 displays the absorption and emission spectra of **1** and **2** in CH$_2$Cl$_2$, and Table 1 collects the main photophysical parameters. The absorption spectra show a broad and strong band in the Vis-NIR spectral region which is red-shifted when going from **1** to **2** (570 nm for **1** and 641 nm for **2**). As well, emission bands are centered *ca.* 800 nm for both compounds in the considered solvent.

According to TD-DFT calculations, the lowest-energy absorption band results from the overlap of the S$_0 \rightarrow$ S$_1$ and S$_0 \rightarrow$ S$_2$ electronic transitions, which are assigned to different combinations of HOMO $\rightarrow$ LUMO and HOMO$-1 \rightarrow$ LUMO one-electron excitations (see Fig. 6); this is in accordance with the structured two-peak profile of the absorption band in **2**. Due to the nearly symmetric structures of these D–A–D systems, HOMO and HOMO-1 energy levels are very close in energy, being delocalized over the branched units (*i.e.*, TPA and vinyl units) while LUMO is delocalized over the π-spacer (*i.e.*, pyran
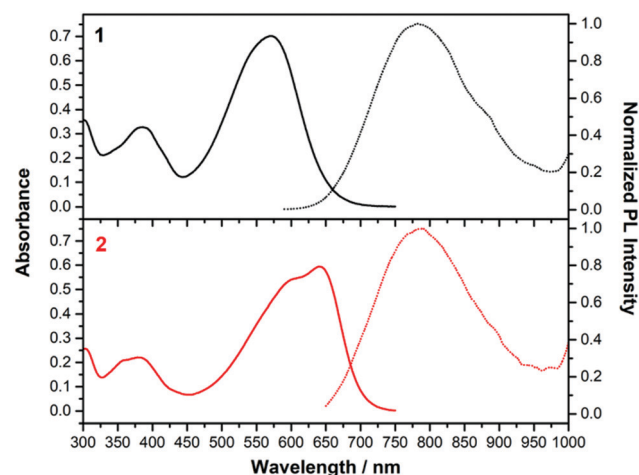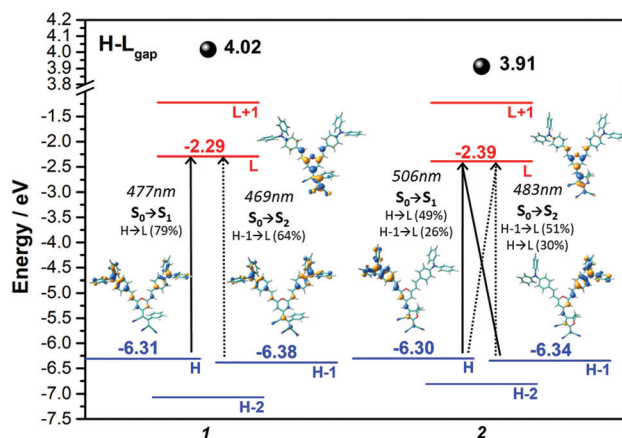

Fig. 6 DFT-calculated frontier molecular orbital energies and topologies for **1** and **2**, at the PCM-M06-2X/6-31G** level using CH$_2$Cl$_2$ as solvent. The S$_0 \rightarrow$ S$_1$ and S$_0 \rightarrow$ S$_2$ electronic transitions are also shown as solid and dashed black arrows, respectively.

and vinyl units) and the acceptor group. Therefore, the S$_0 \rightarrow$ S$_1$ and S$_0 \rightarrow$ S$_2$ electronic transitions imply an electron density redistribution from the peripheral TPA donor units towards the central acceptor group, thus displaying ICT character. Interestingly, the insertion of a stronger acceptor group in **2** causes a lower energy LUMO while the HOMO is slightly affected, thus decreasing the HOMO–LUMO gap, in agreement with the trends shown by the optical gaps (E_g) in Table 1, and with electrochemical data (see Section 4).

Significant Stokes shifts were observed for both chromophores. The differences between the emission fluorescence maxima (λ_{em}) and the lowest-energy electronic absorption maxima (λ_{max}) are 4756 and 2486 cm^{-1} in CH$_2$Cl$_2$ for **1** and **2** respectively. As predicted by TD-DFT (Fig. S8, ESI†), this can be associated to the significant geometrical changes found upon S$_1 \rightarrow$ S$_0$ transition due to the twisted TPA units. This effect is even more pronounced in **1** due to the distorted acceptor group, and a larger Stokes shift is found accordingly.

Furthermore, the absorption and fluorescence emission spectra were studied in different solvents (Fig. S9, ESI†). Both absorption and emission spectra display a marked redshift in parallel to the increase of the solvent polarity, with a more pronounced effect in emission. It is worth noting that large

Fig. 5 Absorption (left, solid line) and emission (right, dashed line) spectra of **1** (black) and **2** (red) in CH$_2$Cl$_2$.

Stokes shifts were appreciated for both compounds regardless of the considered solvent. Treatment of the data according to the Lippert–Mataga equation[44–46] yielded a dipole moment change ($\Delta\mu$) between the ground and the excited state of 19.6 and 15.2 D for **1** and **2** respectively. This is in accordance with the higher dipolar moment calculated in the excited state when compared to the ground state (Table S1, ESI†) and with the stronger positive solvatochromism observed in emission when compared to absorption. This solvent-dependent behaviour denotes the presence of an ICT in these chromophores, and is more outstanding in **2** in line with its more polarized structure; this is in very good agreement with the Raman data and DFT-calculated structural features.

Remarkable photostability in CH_2Cl_2 aerated solutions under the irradiation of UV light was determined for **1** and **2** (Fig. S10, ESI†).[47] In addition, the emission spectra of these chromophores were also examined in different tetrahydrofuran/water mixtures (Fig. S11, ESI†). As the water fraction is higher, a notable increment in the fluorescence intensity was observed for both dyes. This fluorescence enhancement could be ascribed to a combination of intra- and intermolecular effects, since the twisted TPA moieties might restrict the face-to-face intermolecular interactions in the aggregate state favoring the radiative deactivation pathway. These joint features (being dispersable in aqueous media and remaining fluorescent, large Stokes shifts and suitable photostability) suggest potential application of these derivatives in biological fields. Indeed, the utility of compound **1** for confocal fluorescence bioimaging (1P microscopy) in a highly proliferative cell line has been previously reported.[29]

4. Electrochemical studies and spectroelectrochemical Properties

In order to experimentally determine the HOMO and LUMO levels of the chromophores, cyclic voltammetry measurements in CH_2Cl_2 were performed. Similar oxidation potentials with slightly lower reduction potentials are found in **2** with respect to **1**, resulting in similar HOMO levels (−5.64 eV for **1** and −5.65 eV for **2**) and slightly different LUMO levels (−3.88 eV for **1** and −3.93 eV for **2**). This trend is in very good accordance with the DFT-calculated HOMO and LUMO energy levels (see Fig. 6). The unique V-shape structure of the chromophores **1** and **2** containing a central acceptor unit surrounded by two TPA donor units also gives rise to interesting properties regarding intermolecular oxidative coupling reactions. The bridging between TPA units is explored now via either electrochemical or chemical doping approaches. We focus here on the first approach, for the second one see Supporting Information for more details. Both chromophores were electrochemically deposited onto indium tin oxide (ITO) substrates from solutions containing the monomers in CH_2Cl_2. The corresponding cyclic voltammograms recorded during electrodeposition are shown in Fig. 7a and b. The obtained CV data in combination with an observed deposition of material on the working electrode suggests an electrochemical polymerization process between the TPA units of the chromophores.[11,13,14] The increasing peak currents for each
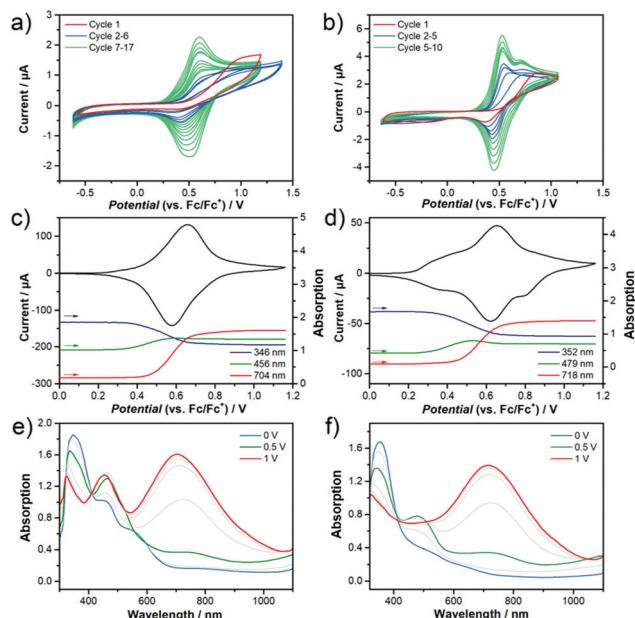

Fig. 7 (a) and (b) Electrochemical oxidative coupling and deposition of **1** and **2** via multiple cycling on ITO substrates (0.1 M TBAPF$_6$ in CH$_2$Cl$_2$, 20 mV s^{-1}, C(monomer) = 0.5 × 10^{-4} mol L^{-1}) to generate cl-**1** and cl-**2**. (c) to (f) In situ spectroelectrochemistry of electrochemically polymerized films on ITO substrates in monomer free solution (0.1 M TBAPF$_6$ in MeCN, 20 mV s^{-1}) of cl-**1** (c) and cl-**2** (d). UV-Vis-NIR absorption spectra during charging cl-**1** (e) and cl-**2** (f), while in (c) and (d) the corresponding evolutions of characteristic absorption bands are given as function of potential. Measurements are performed in a three-electrode setup using Pt as counter electrode and Ag/AgCl as reference electrode.

consecutive cycle can be explained by the increasing amount of redox active material on the electrode.

Fig. 7c–f present the results of spectroelectrochemical measurements of electrochemically polymerized films of **1** and **2**, abbreviated as cl-**1** and cl-**2** in the following in monomer free electrolyte. Both polymer films show fully reversible and stable CVs (Fig. 7c and d). cl-**2** has a higher onset of oxidation when compared to cl-**1**, which can be explained by the stronger electron acceptor group in molecule **2**. While the electrochemical polymerization was performed in CH_2Cl_2 to ensure good solubility of the pure chromophore in the electrolyte, the spectroelectrochemical characterization in monomer free solution displayed in Fig. 7c–f was done in MeCN; thus, the reason for additional features in the CV of cl-**2** in MeCN when compared to that recorded in CH_2Cl_2 might be ascribed to the different polarity of the used electrolytes which can lead to peak splitting in CV.[48,49] Moreover, the individual peaks could also be interpreted in the context of partially interacting redox sites as a consequence to the unique shape of the chromophores having two identical redox groups on each side of the molecule.[50,51] The interaction can cause slight shifts in the oxidation potentials of the individual redox sites, which might interact over the conjugated bridging acceptor unit in the center of the molecular structure.

Fig. 7c and d further display the evolution of absorption intensity of three distinct wavelengths sampled in the

Table 2 Characteristic absorption bands for electrochemically polymerized films of **1** and **2**, denoted as cl-**1** and cl-**2**, and their oxidized species

	$\lambda_{neutral}$ (nm)	$\lambda_{radical\ cation}$ (nm)	$\lambda_{dication}$ (nm)
cl-**1**	346	325, 456	322, 450, 704
cl-**2**	352	343, 479	325, 718

spectroelectrochemical experiment. According to literature[11,13,14] the blue band at around 350 nm can be assigned to a neutral tetraphenylbenzidine (TPB) dimer and the red band at wavelengths above 700 nm to the dication of the TPB dimer. The exact identification of the intermediate radical cation species is difficult since an overlap of absorption signals with the dication complicates a clear assignment for these species. Still, the band at 456 nm (cl-**1**) and 479 nm (cl-**2**) most likely belong to the intermediate radical cation species and are also included in green in the peak evolution graphs. Note that this is also in good agreement with the evolution of the TD-DFT calculated absorption spectra for TPB dimers upon oxidation (Fig. S13, ESI†). All characteristic absorption bands are summarized in Table 2.

At the starting point of the CVs, the neutral band is at maximum absorption confirming the polymer films are in their neutral state (Fig. 7e and f). With increasing electrochemical potential, the neutral band decreases in favor of the green and at higher potentials in favor of the red (dication) band. Following this observation, the films are being transferred from neutral state into the dication passing through an intermediate state herein referred to as radical cation. This process is fully reversed during the reverse scan of the cycle. Still, remaining absorption intensity in the neutral state at wavelengths of 576 nm (cl-**1**) and 663 nm (cl-**2**) at the position of each of the chromophores charge transfer bands indicates that there might be still TPA monomers present in the films (Fig. S13, ESI†). Nevertheless, the spectroelectrochemical measurements prove a successful electrochemical polymerization of both chromophores from solution and help to identify the charged species of the produced TPB dimer units inside the films.

5. Nonlinear optical properties

We now investigate both experimentally and theoretically the molecular second-order NLO response ($\mu\beta$) and the two-photon absorption (2PA) properties of chromophores **1** and **2** in order to establish structure-NLO properties relationships. Finally, we demonstrate the application of these V-shaped chromophores in 2P-excited fluorescence bioimaging (*i.e.*, under two-photon excitation conditions).

5.1 Molecular hyperpolarizabilty

Table 3 collects the second-order NLO properties (*i.e.*, $\mu\beta$ values) of chromophores **1** and **2** measured by electric field-induced second harmonic generation (EFISHG) at 1907 nm in CH_2Cl_2 solution, together with the DFT-calculated data. Zero frequency $\mu\beta_0$ values have been extrapolated by means of the two level model,[52] considering the lowest-energy electronic absorption maxima in CH_2Cl_2 solution (see Table 1). Different electronic transitions contribute to the observed absorption

Table 3 Experimental and calculated molecular hyperpolarizabilities of **1** and **2**

Compound	Experimental		Theoretical
	$\mu\beta^a$ (10^{-48} esu)	$\mu\beta_0^b$ (10^{-48} esu)	$\mu\beta_0^c$ (10^{-48} esu)
1	2550	1490	4871
2	3500	1710	5628

[a] Measured by EFISH in CH_2Cl_2 at 1.9 μm (experimental uncertainty less than ±15%). [b] Experimental $\mu\beta_0$ values calculated using the two level model. [c] Calculated at the M06-2X/6-31G** level in CH_2Cl_2.

bands, therefore $\mu\beta_0$ values thus estimated should be treated with caution. For the sake of comparison, Disperse Red 1 (DR1), a common benchmark for organic NLO chromophores, has been measured under the same experimental conditions as for **1** and **2**. The obtained $\mu\beta_0$ value of *ca.* 510 × 10^{-48} esu is quite close to the value reported for DR1 by Dirk *et al.*[53]

The fact that our chromophores exhibit positive $\mu\beta_0$ values reflects that the contribution of the charge-separated zwitterionic form is higher in the excited state than in the ground state, thus resulting in an increased dipole moment change upon excitation as predicted by TD-DFT calculations (Table S1, ESI†); this is in accordance with the positive solvatochromic behaviour for both chromophores discussed above. Interestingly, compound **2** exhibits a higher $\mu\beta_0$ value than **1** in consonance with the more polarized structure and more efficient ICT character upon the insertion of the stronger electron acceptor TCF group. While theoretical results overestimate the experimental values, they reproduce the observed trends. Finally, it could also be instructive to compare the NLO properties of the compounds herein reported to those of related derivatives, although they are somewhat restricted by the different experimental setups used in the measurements. With these strong polycyano acceptors, only diethylaminophenyl analogues[32] are described, and interestingly, the measured $\mu\beta_0$ value of **2** is larger than that reported for the equivalent.[32] Concerning the influence of the cyano-acceptor on position 4 of the 4*H*-pyranylidene, compounds **1** and **2** present a higher NLO activity that the analogue with a dicyanovinylene end,[54] due to the more efficient electron-withdrawing character for the acceptors used here. On the other hand, chromophores featuring quite different acceptor/donor moieties have been reported with lower[21] or higher $\mu\beta_0$ values.[55]

5.2 Two photon-absorption properties

The 2PA cross-sections of **1** and **2** were investigated between 700 and 1000 nm by the two-photon-excited fluorescence method,[56,57] and are represented in Fig. 8. Accounting the photophysical properties and the prior TD-DFT calculations (Fig. S9 and S17, ESI†), in this spectral region the transitions to the first two excited states can not be observed. Instead, higher excited states are reached upon the biphotonic excitation (see Fig. S19, ESI† for comparison between 1PA and 2PA spectra). Compound **2**, having a more prominent ICT character, shows significant 2PA cross section values of up to 326 and 203 GM at 790 and 890 nm, respectively. Furthermore, 2PA properties are
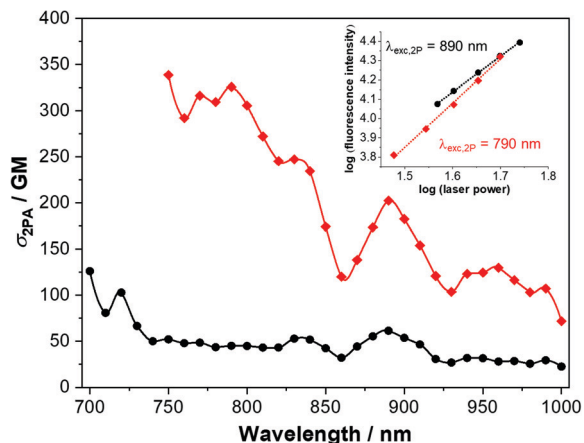
Fig. 8 Two-Photon cross sections (σ_{2PA}) of compounds **1** and **2** (black and red lines correspondingly, 10 μM solutions in toluene). The inset shows the dependence of the two-photon excited fluorescence intensity on the laser power with $\lambda_{exc,2P}$ = 890 nm for **1** and $\lambda_{exc,2P}$ = 790 nm for **2**. The slopes (1.9 (r^2 = 0.9994) and 2.0 (r^2 = 0.9965) for compounds **1** and **2** respectively) are in accordance with the occurrence of two-photon absorption.

Fig. 9 Fluorescence images of subcellular localization of **1** (a–c, $\lambda_{exc,2P}$ = 720 nm, λ_{em} = 450–700 nm) and **2** (d–f, $\lambda_{exc,2P}$ = 740 nm, λ_{em} = 450–700 nm) in MEF cells. (a and d) Brightfield in MEF cells. Fluorescence images of compound **1** (b) and compound **2** (e). Brightfield and fluorescence merged images of compound **1** (c) and compound **2** (f). Scale bar: 15 μm.

even interesting in wavelengths longer than 900 nm, where the cross section is in general above 100 GM. On the other hand, compound **1** displays somewhat reduced 2PA properties when comparing with **2**. However, adequate and remarkable 2PA cross-section values were determined at 720 and 830 nm for this dye (103 and 53 GM respectively). For comparison of our derivatives with other V-shaped compounds with 2PA properties, see Table S3 (ESI†).

The inherent advantages of the 2PA process, derived from the square dependence of the process on the excitation light intensity, can be also exploited in a wide range of solid-related applications, *e.g.*, optical limiting, 3D data storage, microfabrication and so on.[5,58,59] Bearing in mind, we decided to examine the 2PA properties in the cl-**1** and cl-**2** electrochemically polymerized films obtained from the two chromophores under study (Fig. S20 and S21, ESI†). It is worth noting that despite the push–pull systems of the dyes being altered by the polymerization process, the 2P-excited emission is conserved and the biphotonic ocurrence was confirmed in both cases. Interestingly, fluorescence of cl-**2** is blue shifted when compared with that of cl-**1**. Changes in the excitation spectra are also noted, where the 2PA regime is bounded to the region above 800 nm. Thus, these good results seem to indicate that these derivatives, in the polymerized form, are potential candidates to some of the applications mentioned previously.

5.3 Two photon-absorption fluorescence cell imaging

Currently, there is a strong need for organic compounds whose activation takes place in the NIR region of the spectrum with optimal tissue penetration and minimizing background interference and phototoxicity.[5,60–62] The high 2PA cross-sections, large Stokes shift and NIR emission wavelengths of **1** and **2** are clear advantages for their use in biomedical applications. In fact, chromophore **1** was successfully applied for labeling
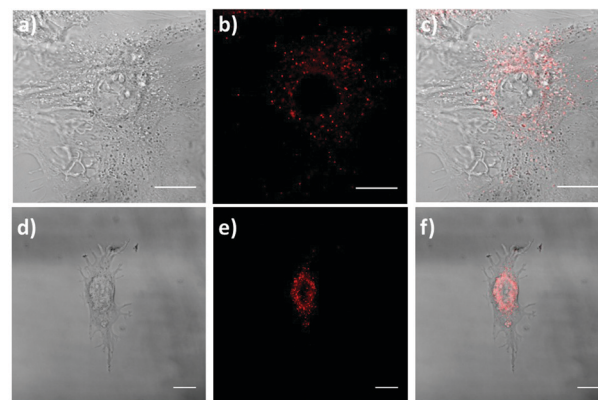
proliferative cells.[29] Since the two-photon properties of **2** are enhanced with respect to **1**, even more interesting results are expected.

For this approach, we selected a healthy cell line consisting of mouse embryonic fibroblast (MEF) cells. The fluorescence properties of chromophores **1** and **2** within living MEFs were analyzed by 2P-microscopy. After incubating MEFs cells with these compounds, these were visualized upon 2P-excitation at 720 and 740 nm respectively, and fluorescence was detected in both cases between 450 nm and 700 nm using a HyD non-descanned detector. As seen in Fig. 9, live treated MEFs with chromophores **1** and **2** exhibited fluorescence at localized cytoplasmic regions. Thus, our results demonstrate that chromophores **1** and **2** are successfully applied as 2P fluorescent probes for bioimaging.

Conclusions

Two V-shaped D–A–D systems with 4*H*-pyranylidene as a part of the π-conjugated bridge, propeller-like TPA donor units, and tricarbonitrile-based acceptor groups have been successfully developed. The two chromophores exhibit interesting photophysical properties (*i.e.*, NIR emission, large Stokes shift, enhanced emission in tetrahydrofuran/water mixtures and good photostability). A slightly larger polarization of the π-conjugated structure is found in chromophore **2** due to the insertion of the TCF acceptor group, as proved by Raman spectroscopy and DFT calculations. In line with this, even more remarkable 2PA cross-section values and molecular first hyperpolarizabilities were found for **2** suggesting their potential for electrooptical and biological applications. In fact, the utility of the two chromophores for two-photon fluorescence bioimaging has been successfully demonstrated. On the other hand, the peculiar electrochemical behavior of these V-shaped chromophores results in the dimerization of the triphenylamino groups to tetraphenylbenzidine upon electrochemical and chemical oxidation.

Importantly, the two-photon excited emission properties are preserved in the polymer films, which highlights their potential for other solid-state applications such as optical limiting, or 3D data storage.

Conflicts of interest

There are no conflicts to declare.

Acknowledgements

References

1 L. R. Dalton, P. A. Sullivan and D. H. Bale, *Chem. Rev.*, 2010, **110**, 25–55.

2 A. Hagfeldt, G. Boschloo, L. Sun, L. Kloo and H. Pettersson, *Chem. Rev.*, 2010, **110**, 6595–6663.

3 K. A. Mazzio and C. K. Luscombe, *Chem. Soc. Rev.*, 2015, **44**, 78–90.

4 Y. Ohmori, *Laser Photonics Rev.*, 2010, **4**, 300–310.

5 M. Pawlicki, H. A. Collins, R. G. Denning and H. L. Anderson, *Angew. Chem., Int. Ed.*, 2009, **48**, 3244–3266.

6 G. Qian and Z. Y. Wang, *Chem. – Asian J.*, 2010, **5**, 1006–1029.

7 M. Klikar, P. Solanke, J. Tydlitát and F. Bureš, *Chem. Rec.*, 2016, **16**, 1886–1905.

8 L. R. Dalton, P. Günter, M. Jazbinsek, O. P. Kwon and P. A. Sullivan, *Organic Electro-Optics and Photonics: Molecules, Polymers, and Crystals*, Cambridge University Press, Cambridge, 2015.

9 Z. Ning and H. Tian, *Chem. Commun.*, 2009, 5483–5495.

10 O. Yurchenko, D. Freytag, L. zur Borg, R. Zentel, J. Heinze and S. Ludwigs, *J. Phys. Chem. B*, 2012, **116**, 30–39.

11 P. Blanchard, C. Malacrida, C. Cabanetos, J. Roncali and S. Ludwigs, *Polym. Int.*, 2019, **68**, 589–606.

12 P. Reinold, K. Bruchlos and S. Ludwigs, *Polym. Chem.*, 2017, **8**, 7351–7359.

13 C. Malacrida, Y. Lu, K. Dirnberger, S. Gámez-Valenzuela, M. C. Ruiz Delgado and S. Ludwigs, *J. Mater. Chem. C*, 2020, **8**, 15393–15405.

14 O. Yurchenko, J. Heinze and S. Ludwigs, *ChemPhysChem*, 2010, **11**, 1637–1640.

15 J. Wang, K. Liu, L. Ma and X. Zhan, *Chem. Rev.*, 2016, **116**, 14675–14725.

16 C. Allain, F. Schmidt, R. Lartia, G. Bordeau, C. Fiorini-Debuisschert, F. Charra, P. Tauc and M.-P. Teulade-Fichou, *ChemBioChem*, 2007, **8**, 424–433.

17 Y. Liu, M. Kong, Q. Zhang, Z. Zhang, H. Zhou, S. Zhang, S. Li, J. Wu and Y. Tian, *J. Mater. Chem. B*, 2014, **2**, 5430–5440.

18 R. Whitby, A. Kay and M. C. Simpson, in *Three-Dimensional Microfabrication Using Two-Photon Polymerization*, ed. T. Baldacchini, William Andrew Publishing, 2nd edn, 2020, pp. 101–141.

19 W. Z. Yuan, Y. Gong, S. Chen, X. Y. Shen, J. W. Y. Lam, P. Lu, Y. Lu, Z. Wang, R. Hu, N. Xie, H. S. Kwok, Y. Zhang, J. Z. Sun and B. Z. Tang, *Chem. Mater.*, 2012, **24**, 1518–1528.

20 R. Andreu, L. Carrasquer, S. Franco, J. Garín, J. Orduna, N. Martínez de Baroja, R. Alicante, B. Villacampa and M. Allain, *J. Org. Chem.*, 2009, **74**, 6647–6657.

21 R. Andreu, E. Galán, J. Garín, V. Herrero, E. Lacarra, J. Orduna, R. Alicante and B. Villacampa, *J. Org. Chem.*, 2010, **75**, 1684–1692.

22 S. G. Awuah, J. Polreis, J. Prakash, Q. Qiao and Y. You, *J. Photochem. Photobiol., A*, 2011, **224**, 116–122.

23 Z. Wang, M. Wang, J. Peng, Y. Xie, M. Liu, W. Gao, Y. Zhou, X. Huang and H. Wu, *J. Phys. Chem. C*, 2019, **123**, 27742–27751.

24 Y. Hong, J. W. Y. Lam and B. Z. Tang, *Chem. Soc. Rev.*, 2011, **40**, 5361–5388.

25 R. Chennoufi, H. Bougherara, N. Gagey-Eilstein, B. Dumat, E. Henry, F. Subra, S. Bury-Moné, F. Mahuteau-Betzer, P. Tauc, M.-P. Teulade-Fichou and E. Deprez, *Sci. Rep.*, 2016, **6**, 21458.

26 M.-X. Liu, L.-L. Ma, X.-Y. Liu, J.-Y. Liu, Z.-L. Lu, R. Liu and L. He, *ACS Appl. Mater. Interfaces*, 2019, **11**, 42975–42987.

27 Y. M. Poronik, V. Hugues, M. Blanchard-Desce and D. T. Gryko, *Chem. – Eur. J.*, 2012, **18**, 9258–9266.

28 M. Jiang, X. Gu, J. W. Y. Lam, Y. Zhang, R. T. K. Kwok, K. S. Wong and B. Z. Tang, *Chem. Sci.*, 2017, **8**, 5440–5446.

29 X. Wang, Z. Guo, S. Zhu, Y. Liu, P. Shi, H. Tian and W.-H. Zhu, *J. Mater. Chem. B*, 2016, **4**, 4683–4689.

30 S. Alías, R. Andreu, M. J. Blesa, S. Franco, J. Garín, A. Gragera, J. Orduna, P. Romero, B. Villacampa and M. Allain, *J. Org. Chem.*, 2007, **72**, 6440–6446.

31 G. Melikian, F. P. Rouessac and C. Alexandre, *Synth. Commun.*, 1995, **25**, 3045–3051.

32 R. Andreu, L. Carrasquer, J. Garín, M. J. Modrego, J. Orduna, R. Alicante, B. Villacampa and M. Allain, *Tetrahedron Lett.*, 2009, **50**, 2920–2924.

33 C. Dehu, F. Meyers and J. L. Brédas, *J. Am. Chem. Soc.*, 1993, **115**, 6198–6206.

34 D. Chasseau, J. Gaultier, C. Hauw, R. Fugnitto, V. Gianis and H. Strzelecka, *Acta Crystallogr., Sect. B: Struct. Crystallogr. Cryst. Chem.*, 1982, **38**, 1629–1631.

35 N. Martínez de Baroja, J. Garín, J. Orduna, R. Andreu, M. J. Blesa, B. Villacampa, R. Alicante and S. Franco, *J. Org. Chem.*, 2012, **77**, 4634–4644.

36 E. Galán, R. Andreu, J. Garín, L. Mosteo, J. Orduna, B. Villacampa and B. E. Diosdado, *Tetrahedron*, 2012, **68**, 6427–6437.

37 A. B. Marco, N. Martínez de Baroja, S. Franco, J. Garín, J. Orduna, B. Villacampa, A. Revuelto and R. Andreu, *Chem. – Asian J.*, 2015, **10**, 188–197.

38 M. C. Ruiz Delgado, J. Casado, V. Hernández, J. T. López Navarrete, J. Orduna, B. Villacampa, R. Alicante, J.-M. Raimundo, P. Blanchard and J. Roncali, *J. Phys. Chem. C*, 2008, **112**, 3109–3120.

39 J. Casado, M. C. Ruiz Delgado, M. C. Rey Merchán, V. Hernández, J. T. López Navarrete, T. M. Pappenfus, N. Williams, W. J. Stegner, J. C. Johnson, B. A. Edlund, D. E. Janzen, K. R. Mann, J. Orduna and B. Villacampa, *Chem. – Eur. J.*, 2006, **12**, 5458–5470.

40 C. C. Ferrón, M. C. Ruiz Delgado, O. Gidron, S. Sharma, D. Sheberla, Y. Sheynin, M. Bendikov, J. T. López Navarrete and V. Hernández, *Chem. Commun.*, 2012, **48**, 6732–6734.

41 T. Takenaka, *Spectrochim. Acta, Part A*, 1971, **27**, 1735–1752.

42 A. Girlando and C. Pecile, *Spectrochim. Acta, Part A*, 1973, **29**, 1859–1878.

43 M. S. Khatkale and J. P. Devlin, *J. Chem. Phys.*, 1979, **70**, 1851–1859.

44 E. Lippert, *Z. Naturforsch., A: Phys. Sci.*, 1955, **10**, 541–545.

45 N. Mataga, Y. Kaifu and M. Koizumi, *Bull. Chem. Soc. Jpn.*, 1955, **28**, 690–691.

46 N. Mataga, Y. Kaifu and M. Koizumi, *Bull. Chem. Soc. Jpn.*, 1956, **29**, 465–470.

47 Note that compound 1 was previously demonstrated to display better photoestability to that recorded to the commercially NIR dye ICG. See ref. 29.

48 S. Arnaboldi, T. Benincori, A. Penoni, L. Vaghi, R. Cirilli, S. Abbate, G. Longhi, G. Mazzeo, S. Grecchi, M. Panigati and P. R. Mussini, *Chem. Sci.*, 2019, **10**, 2708–2717.

49 C. Malacrida, A. H. Habibi, S. Gámez-Valenzuela, I. Lenko, P. Simón Marqués, A. Labrunie, J. Grolleau, J. T. López Navarrete, M. C. Ruiz Delgado, C. Cabanetos, P. Blanchard and S. Ludwigs, *ChemElectroChem*, 2019, **6**, 4215–4228.

50 E. Quartapelle Procopio, T. Benincori, G. Appoloni, P. R. Mussini, S. Arnaboldi, C. Carbonera, R. Cirilli, A. Cominetti, L. Longo, R. Martinazzo, M. Panigati and R. Pò, *New J. Chem.*, 2017, **41**, 10009–10019.

51 M. Hasegawa, K. Kobayakawa, H. Matsuzawa, T. Nishinaga, T. Hirose, K. Sako and Y. Mazaki, *Chem. – Eur. J.*, 2017, **23**, 3267–3271.

52 D. R. Kanis, M. A. Ratner and T. J. Marks, *Chem. Rev.*, 1994, **94**, 195–242.

53 C. W. Dirk, H. E. Katz, M. L. Schilling and L. A. King, *Chem. Mater.*, 1990, **2**, 700–705.

54 C. R. Moylan, S. Ermer, S. M. Lovejoy, I. H. McComb, D. S. Leung, R. Wortmann, P. Krdmer and R. J. Twieg, *J. Am. Chem. Soc.*, 1996, **118**, 12950–12955.

55 S.-S. P. Chou and C.-Y. Yu, *Synth. Met.*, 2004, **142**, 259–262.

56 F. Terenziani, C. Katan, E. Badaeva, S. Tretiak and M. Blanchard-Desce, *Adv. Mater.*, 2008, **20**, 4641–4678.

57 M. Rumi and J. W. Perry, *Adv. Opt. Photon.*, 2010, **2**, 451–518.

58 S. R. M. A. K.-S. Lee, *Photoresponsive Polymers I*, Springer, Berlin, Heidelberg, 1st edn, 2008.

59 G. S. He, L.-S. Tan, Q. Zheng and P. N. Prasad, *Chem. Rev.*, 2008, **108**, 1245–1330.

60 C. Benitez-Martin, J. A. Guadix, J. R. Pearson, F. Najera, J. M. Perez-Pomares and E. Perez-Inestrosa, *Sens. Actuators, B*, 2019, **284**, 744–750.

61 C. Benitez-Martin, J. A. Guadix, J. R. Pearson, F. Najera, J. M. Perez-Pomares and E. Perez-Inestrosa, *ACS Sens.*, 2020, **5**, 1068–1074.

62 C. S. Lim and B. R. Cho, *Tetrahedron*, 2015, **71**, 8219–8249.